Direct measurement of the built-in potential in a nanoscale heterostructure

Anna M. Zaniewski,[1,2,3] Matthias Loster,[1,2] Bryce Sadtler,[4,2,*] A. Paul Alivisatos,[4,2] and A. Zettl[1,2,3,†]

[1]*Department of Physics, University of California at Berkeley, Berkeley, California 94720, USA*

[2]*Materials Sciences Division, Lawrence Berkeley National Laboratory, Berkeley, California 94720, USA*

[3]*Center of Integrated Nanomechanical Systems, University of California at Berkeley, Berkeley, California 94720, USA*

[4]*Department of Chemistry, University of California at Berkeley, Berkeley, California 94720, USA*

(Received 13 July 2010; revised manuscript received 16 September 2010; published 13 October 2010)

We combine transmission electron microscopy with electrostatic force microscopy to determine the built-in potential across individual isolated Cu_2S-CdS heterostructured nanorods. We observe a variation of potentials for different bicomponent nanorods, ranging from 100 to 920 mV with an average of 250 mV. Nanorods of a uniform composition with no heterojunction do not show a built-in potential, as expected. The results are particularly relevant for applications of colloidal nanocrystals in optoelectronic devices such as photovoltaics.

The electronic structure of nanocrystals is an intriguing basic science topic and of great importance for applications. However, few experimental techniques exist to directly characterize on a nanometer scale the electronic properties of structurally well-characterized heterogeneous materials. In fact, one of the most important characteristics of a semiconductor-semiconductor interface, the built-in potential, which determines the suitability of the interface for charge rectifying applications such as photovoltaics, has not previously been directly measured for an isolated bicomponent nanorod (NR). As colloidally grown nanocrystals typically display a distribution of properties, single-particle measurements are invaluable for observing individual differences.[1] In the bicomponent cuprous sulfide—cadmium sulfide (Cu_2S-CdS) heterojunction NRs examined in this work, there is significant variability in the relative fraction of the two materials among individual NRs, even within a given batch. Ideally, one would like to correlate the internal chemical structure of the NR with an independent mapping of the electronic structure of the *same* NR.

We report such a correlation experiment here. We use high-resolution transmission electron microscopy (TEM) to characterize Cu_2S-CdS NRs and then employ electrostatic

force microscopy (EFM), an adaptation of atomic force microscopy (AFM), to determine the electrostatic potential gradient associated with the same NRs. This is the first such application of EFM. EFM has previously been successfully employed to characterize semiconductors and nanomaterials including the charging of nanoscale systems,[2–4] polarization in the tip-sample direction,[5] and resolving surface potential distributions on thin films.[6,7] Another technique for classifying nanomaterials, scanning tunneling spectroscopy, has been used to measure the band offsets of heterogeneous nanocrystals.[8–10] In this study we find that homogeneous, single-component NRs with no heterojunction display no built-in potential, while bicomponent NRs have a built-in potential ranging from 100 to 920 mV. For comparison, a Cu_2S-CdS thin film has a built-in potential of 840 mV and exhibits photovoltaic behavior.[11,12] Additionally, the polarity of the built-in voltage for all bicomponent NRs studied is consistent with a Cu_2S-CdS thin film, that is, the CdS side is negative and the Cu_2S side is positive.

Cu_2S-CdS NRs were synthesized using partial cation exchange to substitute Cu^+ for Cd^{2+} ions within CdS NRs, as described previously.[13] The exchange reaction leads to separate regions of Cu_2S and CdS connected by well-defined,
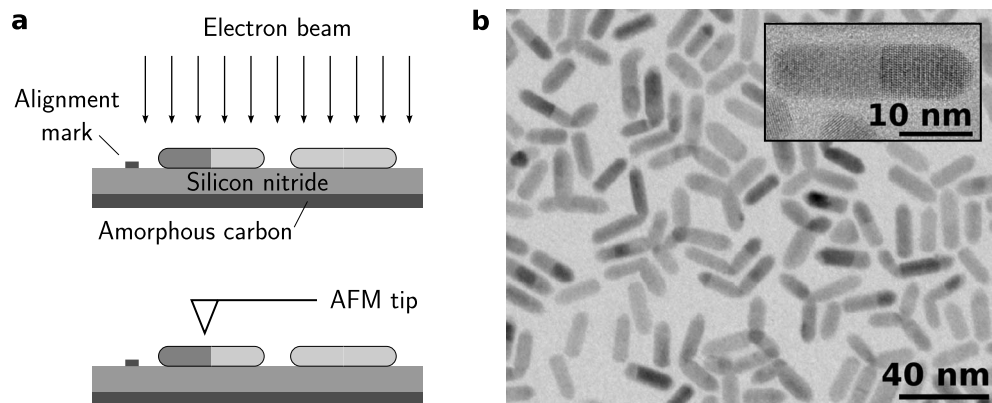

FIG. 1. (a) A schematic of the experiment. The rods are examined in the TEM on an electron transparent silicon nitride window with a thin rear coating of conducting amorphous carbon. This substrate enables the same rods to be imaged with both the TEM for heterojunction identification and electrostatic force microscopy, which requires a conducting back plane. (b) High-resolution TEM image of CdS-Cu_2S nanorods on a carbon film substrate. In the high magnification inset, lattice planes of both materials are visible, and the two materials induce a contrast difference over the length of the rod. Note that not all rods display a heterojunction.
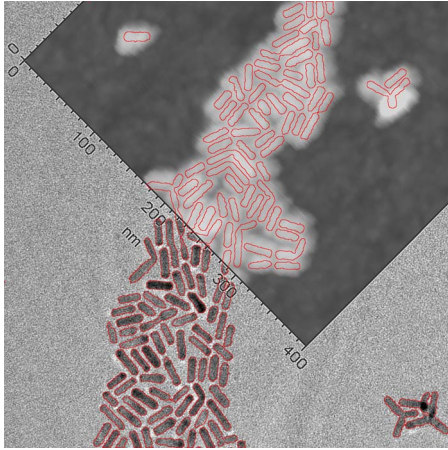
FIG. 2. (Color online) AFM topography image (upper right) overlaid upon a TEM image of the same sample of CdS-Cu$_2$S NRs. The outlines of the rods (red online) are determined by the TEM image. Each line in the AFM image was consecutively scanned for topography and EFM measurements. The topography scan data are used to determine the boundaries of the rods and the TEM data are used to determine the presence and orientation of a heterostructure for EFM analysis.

epitaxial interfaces.[14] The NRs used in this study have an average length of 29 ± 4 nm and an average diameter of 9 ± 4 nm; there is little change in the NR dimensions upon the partial transformation to Cu$_2$S.

The Cu$_2$S-CdS NRs were spin coated under argon upon a silicon nitride substrate with alignment marks and 20-nm-thick windows with 10 nm of amorphous carbon on the backside. This carbon layer provides a grounding plane for the EFM measurements while maintaining electron transparency. A control sample batch with homogeneous CdS rods that had not undergone exchange was prepared in the same fashion. TEM images were obtained with a JEOL 2010 TEM

operated at 100 keV and AFM/EFM measurements were obtained with an Asylum Research MFP-3D AFM with platinum coated silicon probes (Olympus OMCL-AC240TM) under continuous argon flow at 1.5 sccm/s.

Figure 1 a shows schematically the experimental sample measurement configuration. Figure 1(b) shows TEM images for bicomponent Cu$_2$S-CdS NRs and the inset shows a high-resolution image of a single NR heterostructure. The bicomponent nature of this NR is dramatically evident with contrasting lattice planes clearly defining a heterojunction approximately halfway across the length of the rod. At lower resolution the bicomponent nature of most of the NRs is still evident, as shown by the TEM contrast differential across the NRs in the main panel of Fig. 1(b). Importantly, not all of the rods examined display a heterojunction.

Alignment marks on the sample substrate allow individual NRs characterized by TEM to be subsequently located and characterized by AFM/EFM. Figure 2 shows an example of the dual-measurement and correlation method. The lower portion of the figure shows a TEM image of ion-exchanged Cu$_2$S-CdS NRs with the outer perimeters highlighted for clarity (red online). In the upper portion of Fig. 2, similar TEM data exist, but only the perimeters of the NRs have been drawn. The upper portion of Fig. 2 represents AFM topography data. Because of small thermal drift during the relatively slow AFM scan the AFM topography image is registered by an affine transformation using three landmark points.

The low-resolution AFM topography data shown in Fig. 2 serve only to register the AFM instrument to predetermined NR locations. At specific locations of TEM-characterized NRs, EFM data were collected. For EFM measurements, a conducting AFM tip was used to scan each line of the sample twice, first near the surface for topography, and then raised 20 nm above the surface with a bias dc voltage applied to the tip. During the raised scan, the electrostatic interaction be-
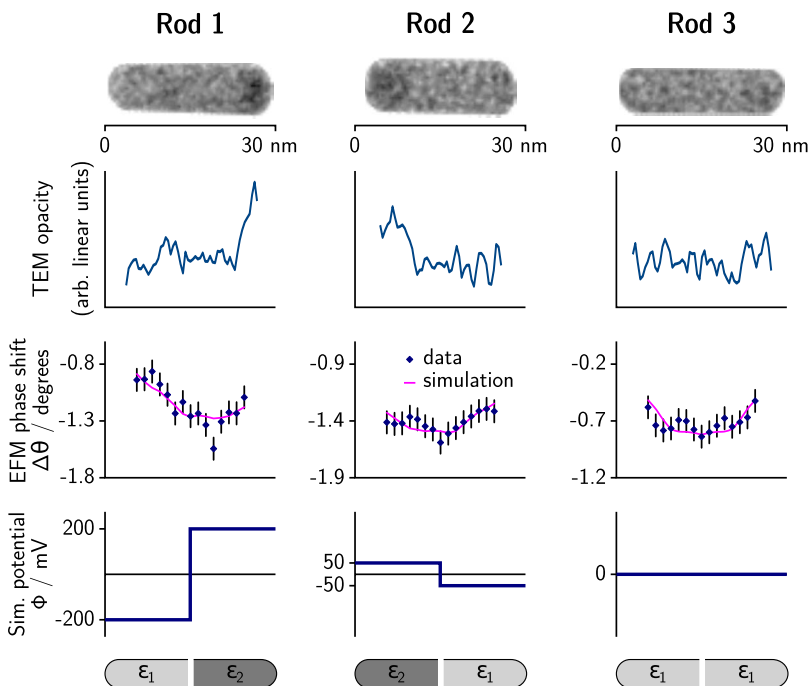

FIG. 3. (Color online) Top: TEM images and opacity profiles of rods (1) and (2) which reveal a heterojunction and rod (3) which does not. Middle: EFM data (phase shift cross sections) which are asymmetric in rods (1) and (2) but not in (3). The lines through the EFM data are the results of a finite-element electrostatic calculation modeling the tip/CdS-Cu2S rod/substrate system. Bottom: in the model, the heterojunction is represented by strips held at $-V_{bi,sim}/2$ and $V_{bi,sim}/2$, and dielectric constants are set to the bulk values. For (1), V_{bi} =400 mV and for (2), V_{bi} =100 mV. The symmetric rod (3) fits best to V_{bi}=0 V with the same dielectric constant for each side.

TABLE I. Statistical analysis of EFM data. Shown are the slope of the phase shift trend over the rod, normalized to the length of the rod, V_{bi} and the reduced χ^2 goodness of fit parameter for this V_{bi}. The first three rows present the results for rods (1), (2), and (3) shown in Fig. 3. The fourth row gives the averages of the results for all rods. In the fifth row, all phase profiles were averaged before they were analyzed as a single data set. The last row shows the average results for the single material CdS control rods.

	$\Delta\Theta/\Delta x$ (mdeg/nm)	Best V_{bi} fit (mV)	Reduced χ^2
Rod(1)	12	400	0.96
Rod(2)	9	100	0.5
Rod(3)	1.4	0	0.64
Averaged results	14 ± 9	250	0.96
Averaged data for each position	15	100	1.4
Control CdS rods	3.2 ± 2.8	0	1.04

tween the sample and the tip causes a phase shift in the signal[15]

$$\Delta\Theta = \arcsin\left(\frac{Q}{k}\frac{dF}{dz}\right), \quad (1)$$

where Q is the quality factor of the cantilever, k is the spring constant, and dF/dz is the derivative of the force with respect to the tip-sample distance.

Figure 3 shows, for three independent NRs, the raw TEM image (upper row images) along with the TEM opacity, obtained by measuring the contrast level along a central axis line scan of the NR. The TEM opacity is shown in the second row of Fig. 3. The TEM images and opacity line scans clearly indicate a nonhomogeneous nature to NRs 1 and 2. The darker region (on the right side of NR 1, and on the left side of NR 2) is identified with Cu$_2$S while the lighter region is identified with CdS.[13] Hence, NRs 1 and 2 are bicomponent NRs (though apparently not with 50/50 composition distributions) with expected built-in electrostatic potentials. NR 3, on the other hand, has relatively uniform TEM contrast (even though it was a member of the ion-exchanged batch). For each NR, the experimentally determined $\Delta\Theta$ EFM data yield the electrostatic potential difference, $\phi_{left} - \phi_{right}$, across the NR heterostructure. We caution that $\Delta\Theta$ and ϕ are related but not trivially so. Due to the alignment of the Fermi levels at the interface between the two components in the bicomponent Cu$_2$S-CdS NRs, a space charge region is formed that induces a built-in voltage across the NRs. Theoretical work has shown that on the scale of tens of nanometers, EFM resolution will be limited and the signal $\Delta\Theta$ does not emulate precisely the shape of the surface potential.[16] In fact, the measured force gradient arises from a convolution of forces in the tip-sample-substrate system. To correctly extract ϕ from the experimental data, three-dimensional modeling must be employed. We do not quote a spatial resolution for our EFM measurements since at this scale the phase profile across the NR is more meaningful than the measurement at a single point. We demonstrate that we can use this phase profile to extract the built-in potential across the NRs.

To correlate the measured phase shift $\Delta\Theta$ profile with the built-in potential of the NRs, $\phi_{left} - \phi_{right} = V_{bi}$, we generated a three-dimensional finite-element model with COMSOL. The

AFM tip was modeled as a cone with a spherical apex with dimensions given by the manufacturer and was positioned above a single NR. We did not include the cantilever in the model, as it has been shown to have negligible influence on the phase shift profile.[5] The NR on the substrate surface was modeled as two separate, adjoining strips with dielectric constants ϵ_1 and ϵ_2 set to the bulk values for CdS and Cu$_2$S. The model strips were separated by a 1 nm gap and kept at $-V_{bi,sim}/2$ and $V_{bi,sim}/2$, respectively, where $V_{bi,sim}$ was varied from 0 to 1 V. The gap avoids divergence during computation and is expected to have negligible influence on the result. For simplicity, we modeled the two component sides as equal in length.[17]

Using the model, the electrostatic force between the tip and the sample was calculated for a series of tip positions along the NR axis and at three different tip heights above the sample, at 19, 20, and 21 nm. To obtain the force gradient at each position along the NR, we used a finite difference approximation. With the forces from the three different tip heights we calculated two gradients and ensured that they converge to better than 10%. Using the measured values for Q and k, and Eq. (1), we generated the expected phase shift.

Figure 3 shows, in the third row, the experimentally determined EFM $\Delta\Theta$ data for NRs 1, 2, and 3. The solid lines represent $\Delta\Theta$ as predicted by the model, for the ϕ and dielectric constant distributions shown in the fourth and last rows of Fig. 3. Interestingly, we find that NRs 1 and 2 have different built-in potential magnitudes, 400 mV and 100 mV, respectively. As expected, the polarity of the built-in potential is correlated with the TEM determined structural composition. In contrast, NR 3, which has no TEM visible junction, fits best to a flat electrostatic potential.

To confirm the reliability of the modeling to extract V_{bi} from $\Delta\Theta$, checks were preformed on an idealized bicomponent control nanorod consisting of a 40 nm wide and 30-nm-thick gold line with a gap of 20 nm in the center. The line was drawn with electron beam lithography on a similar substrate as used for the NRs. Each side of the line was connected to a tunable voltage source, allowing us to control the potential difference across the structure. We then performed EFM measurements on this system, and verified that our model, adjusted to reflect the geometry of this control system, accurately reproduced the phase shift response to a

known potential difference, equivalent to the built-in voltage in a NR.

Additional NRs were examined in a manner similar to that described for the three specimens in Fig. 3. EFM analysis of a control batch of 27 nonion-exchanged CdS NRs resulted in flat electrostatic potentials, i.e., $V_{bi}=0$. TEM and EFM measurements were performed on 18 additional bicomponent Cu_2S-CdS NR specimens which showed a single junction in TEM analysis and had random physical orientations. The results for these additional samples, together with those for NRs 1, 2, and 3, and the control CdS set, are summarized in Table I.

Table I shows that the phase gradient $d\phi/dx$ (and thus the built in potential) has the same polarity for all 20 bistructure NRs; using TEM opacity measurements, we determined that the phase gradient increases from the CdS side to the Cu_2S side. The average slope is $0.014°/nm$ with a standard deviation of 0.0097. For comparison, the average of the absolute value of the slope of a control batch of 27 pure CdS rods is $0.003°/nm$, indicating that the measured gradients of the bicomponent rods are within our measurement resolution.

The average built-in potential for the NRs is $\langle V_{bi}\rangle$ $=250$ mV. Excluded from this set are 3 NRs which had poor fits to the model (reduced $\chi^2 > 1.6$).[18] For the χ^2 analysis, we use the EFM error of 0.1°, based on measurements over the empty substrate. The average goodness of fit for this set is $\langle \chi^2 \rangle = 0.96$, and the average χ^2 for all 20 rods is 1.1, indicating good consistency between the model and the experiment. We estimate the error of determining the built-in voltage with our method to be ± 100 mV, an interval within which the χ^2 goodness of fit values do not clearly favor a specific value for V_{bi}.

In addition to analyzing individual rods, we also analyzed the average phase profile of all NRs, by aligning orientationally all 20 EFM profiles and averaging. Table I (fifth row) shows the results for this averaged profile, which compares well with taking the average of the individually fitted NRs: the slopes are similar and V_{bi} is within the expected error margin.

Table II gives the distribution of built-in potentials associated with the NRs. Ten of the twenty NRs have a V_{bi} in the range 100 ± 100 mV while seven have a larger V_{bi} of up to

TABLE II. The number of rods associated with each V_{bi} interval, as determined by a χ^2 analysis of the fit of the measured phase profiles to the model. For three of the twenty NRs, χ^2 values did not indicate a good fit.

V_{bi}	Number of rods
<200 mV	10
200–400 mV	2
400–600 mV	2
600–920 mV	3
Min $\chi^2 > 1.6$ (poor fit)	3

920 mV. No NR has a potential greater than 920 mV. The voltage variation within the set may arise from: the presence of different crystalline phases of Cu_2S (high chalcocite, low chalcocite, or djuerlite); lattice plane orientation at the CdS-Cu_2S interface; or the presence of a small Cu_2S cap at the end of the CdS portion of the rod. Despite clearly identifying NRs with a junction, the TEM images do not reveal these small variations that can cause the observed variability in the phase profile and the resulting built-in potential.

In summary, we measured electrostatic potential gradients in nanorods with a technique that is sensitive to the individual variability in the built-in potentials of the rods. Most rods examined showed a built-in potential in the range of 100–400 mV, with some as high as 920 ± 100 mV, indicating that these rods show promise for applications such as photovoltaics. The characterization technique is generally useful to electronically quantify new nanostructured materials.

*Present address: Division of Chemistry and Chemical Engineering, California Institute of Technology, Pasadena, CA 91125, USA.

†azettl@berkeley.edu

[1] S. Empedocles and M. Bawendi, Acc. Chem. Res. **32**, 389 (1999).

[2] R. Costi, G. Cohen, A. Salant, E. Rabani, and U. Banin, Nano Lett. **9**, 2031 (2009).

[3] R. Krishnan, M. A. Hahn, Z. Yu, J. Silcox, P. M. Fauchet, and T. D. Krauss, Phys. Rev. Lett. **92**, 216803 (2004).

[4] O. Cherniavskaya, L. Chen, M. A. Islam, and L. Brus, Nano Lett. **3**, 497 (2003).

[5] O. Cherniavskaya, L. Chen, V. Weng, L. Yuditsky, and L. E. Brus, J. Phys. Chem. B **107**, 1525 (2003).

[6] A. Kikukawa, S. Hosaka, and R. Imura, Appl. Phys. Lett. **66**, 3510 (1995).

[7] H. Hoppe, T. Glatzel, M. Niggemann, A. Hinsch, M. C. Lux-Steiner, and N. S. Sariciftci, Nano Lett. **5**, 269 (2005).

[8] U. Banin, Y. Cao, D. Katz, and O. Millo, Nature (London) **400**, 542 (1999).

[9] D. Steiner, T. Mokari, U. Banin, and O. Millo, Phys. Rev. Lett. **95**, 056805 (2005).

[10] D. Steiner, D. Dorfs, U. Banin, F. D. Sala, L. Manna, and O. Millo, Nano Lett. **8**, 2954 (2008).

[11] S. M. Sze, *Physics of Semiconductor Devices* (Wiley, New York, 1981).

[12] H. W. Brandhorst, NASA Technical Report No. D-5079, 1969 (unpublished).

[13] B. Sadtler, D. O. Demchenko, H. Zheng, S. M. Hughes, M. G. Merkle, U. Dahmen, L.-W. Wang, and A. P. Alivisatos, J. Am. Chem. Soc. **131**, 5285 (2009).

[14] The average fraction of Cu_2S depends on the number of Cu^+ cations added to the batch. The relative fraction of Cu_2S varies among individuals within a sample. The growth of Cu_2S into the CdS NRs via cation exchange preferentially occurs at the end facets leading to Cu_2S segments at one or both ends. The interface between the segments, though not apparent in Fig. 3, can be studied with high-resolution TEM and is discussed in detail in Ref. 13.

[15] P. Samorì, *Scanning Probe Microscopies Beyond Imaging* (Wiley-VCH, Weinheim, Germany, 2006).

[16] Y. Shen, M. Lee, W. Lee, D. M. Barnett, P. M. Pinsky, and F. B. Prinz, Nanotechnology **19**, 035710 (2008).

[17] We find that this approximation, which is obviously not precisely correct for NRs 1 and 2, introduces only a modest deviation within an estimated range of ± 100 mV in the determination of V_{bi}; the limited EFM resolution on this scale does not justify a more complex component distribution.

[18] The phase profile trends for these rods are similar to the trend in all other rods but the fits are poor because these NRs include statistical variations that are larger than average. For normal statistical fluctuations, the probability of measuring three or more rods with a χ^2 value greater than 1.6 is 32%, given our sample size of 20. Thus, the presence of three rods with a poor fit to the model is indicative of expected statistical variations.